In-situ analysis of steelmaking slags and mold fluxes at elevated temperatures using a remote fiber-optic Raman probe

H. Tekle[1], B. Zhang[2], T. Sander[3], J. D. Smith[4], R. E. Gerald II[5], J. Huang[6], R. J. O'Malley[7]

1. Graduate Student, Missouri University of Science and Technology, Rolla, Missouri, 65409 hwtr29@mst.edu
2. Assistant Research Professor, Missouri University of Science and Technology, Rolla, Missouri, 65409. bzdtx@mst.edu
3. Lab Specialist, Missouri University of Science and Technology, Rolla, Missouri, 65409. tpsand@mst.edu
4. Professor, Missouri University of Science and Technology, Rolla, Missouri, 65409. jsmith@mst.edu
5. Research Professor, Missouri University of Science and Technology, Rolla, Missouri, 65409. geraldr@mst.edu
6. Associate Professor, Missouri University of Science and Technology, Rolla, Missouri, 65409. jieh@mst.edu
7. Professor, Missouri University of Science and Technology, Rolla, Missouri, 65409. omalleyr@mst.edu

Keywords: Fibre-optic sensor, Raman spectroscopy, *in-situ* Raman, high-temperature Raman spectroscopy, real time analysis, steelmaking slag, mold flux.

ABSTRACT

In the steelmaking process, mold fluxes are essential for ensuring thermal insulation, refining, and the efficiency of continuous casting. Real-time understanding of the in-service composition of slags and fluxes are crucial for optimizing the steel production process and improving the quality of the final product. An *in-situ* fibre-optic Raman probe that enables the study of the structure, composition, and viscosity of molten slags and fluxes at steelmaking temperatures has been developed and demonstrated both in the lab and in foundry scale experiments. The focus of this study is on the structural, compositional, and property analysis of molten fluxes in a laboratory setting, with the aim of applying this technology for *in-situ* monitoring during industrial production. Raman spectra were successfully collected at various temperatures from 1000°C to 1400°C in real-time and analysed using a deconvolution algorithm to isolate and quantify peaks in the spectra associated with the specific structures of molecular components in molten and solidifying flux. The research successfully combines *in-situ* Raman spectroscopy with high-temperature viscosity data, specifically targeting CaO-CaF-SiO_2-Al_2O_3 based mould flux systems. Specified ratios of the deconvoluted Raman peaks, such as Al-O-Al/Si-O-Si ratio, shows good correlation with the flux chemistry, while the Q^3/Q^0 peak ratio shows good correlation with viscosity. A ruggedized Raman probe system was also developed and demonstrated in an 80 kg induction furnace. Ultimately, the goal of this work is to demonstrate *in-situ* slag and mould flux analysis in industrial processes, such as in the continuous caster or electric arc furnace (EAF).

INTRODUCTION

In steelmaking, the significance of slags and fluxes cannot be overstated. They are an integral component of the steelmaking process that are required to ensure product quality and process efficiency. As elucidated in studies by Mills, K.C. (2016) and Pretorius, E.B. (2020), fluxes and slags serve many roles in the production of steel. In the continuous casting process, mold fluxes create a protective slag film that prevents the molten steel from adhering to the mold and plays a pivotal role in thermal insulation, surface lubrication, inclusion absorption, and in managing the growth of the solidifying steel shell. In the Electric Arc Furnace (EAF), slag composition is managed to maintain a target basicity and MgO supersaturation level to protect the refractory and promote slag foaming and phosphorous removal. Control of the slag composition during oxygen blowing and FeO generation is essential for sustaining a foamy slag practice conducive to efficient high-power EAF operations. Similarly, in continuous casting, mold flux must be designed to account for inclusion absorption and exchange reactions with the steel when reactive elements in the steel are present. These changes in composition affect the properties of the flux during the casting process, often degrading the functionality of the flux over time. Min, D.J. and Jung, S.B. (2016) underscore the importance of slag composition and viscosity in metallurgical processes. Slags can undergo substantial compositional shifts due to the addition of various constituents throughout the steelmaking process. These additions affect the physicochemical properties of the slag, thereby influencing their behaviour and efficacy in steelmaking. In each of these scenarios, whether in the EAF or during continuous casting, *in-situ* determination of the in-service composition of the slag or flux would be invaluable. Such knowledge would provide insights into the current state of the process and opens the possibility for

dynamic composition adjustments during operation. This real-time monitoring and adjustment capability could significantly enhance process control, leading to better quality steel production with optimized efficiency.

Raman spectroscopy has been demonstrated to provide useful information about the composition and structure of slags, glasses, and fluxes used in metallurgical processes. Most investigations have focused on Raman spectra measurements on quenched materials at room temperature. A recent study investigated the structure and viscosity of quenched $CaO\text{-}SiO_2\text{-}Fe_XO$ slags during the early stages of basic oxygen steelmaking by Zhang, R. et al. (2020). Their research showed that Raman spectroscopy can effectively analyse the glassy samples of different slag systems, shedding light on the proportion of various silicate and iron structures. By tracking the coordination of Fe^{3+} transformations from octahedron to tetrahedron, the provided O^{2-} was shown to contribute to the depolymerization of the silicate network. The information found on bridging and nonbridging oxides was incorporated into a viscosity estimation equation that showed a 20% error when comparing estimations to actual measurements. Gyakwaa, F. et al. (2019, 2020, 2020c) demonstrated the applicability of time-gated Raman spectroscopy in characterizing calcium-aluminate inclusions in steel. In separate studies, from Gyakwaa, F. et al. (2020a, 2020b), showcased how Raman spectroscopy can be used to estimate phase fractions for duplex oxide-sulphide inclusions, providing valuable information about their composition and structure. In addition, the use of the relative Raman peak intensities produced good correlations with phase fractions of CaS phases. Gao, J. et al. (2016, 2016a) highlighted the use of Raman spectroscopy in understanding the structure and crystallization behaviour of various alumina and silica mold fluxes and slags. They found that increased Al-O-Al and Si-O-Al peaks were indicative of depolymerizing behaviour of the silica network. Chen, H. et al. (2016) leveraged Raman spectroscopy to analyse the structure of mold flux by indexing the degree of polymerization and correlating that to basicity and activation energy of the silicate melt. As such, by understanding relative quantities of molecular bonds, inferences can be made about the structure and properties of the material. Raman spectroscopy provides insights into the degree of polymerization and the distribution of various polymerized silicate and aluminosilicate structures within the slag, which are key determinants of structure.

McMillan, P.F. et al. (1994), Daniel, I. et al. (1995), and Malfait, W.J., et al. (2007, 2008) have performed Raman measurements at elevated temperatures using hot wire or hot stages systems demonstrating the viability of performing high-temperature Raman analysis. The works show the temperature sensitivity of Raman. McMillan, P.F. et al. (1994) showed that the silica melts relaxed due to the breakage of Si-O-Si bonds and was consistent with viscosity. In addition, they attribute Raman peak shifts to the decreasing Si-O-Si bond angle as temperature was increased. The primary barrier to implementation of high temperature *in-situ* Raman spectroscopy in the production environment stems from the limitations of the existing benchtop systems. To address this, an enhanced configuration has been developed by Zhang, B., et al. (2023). This fibre-optic Raman system boasts significant advantages, such as its portability due to a smaller form factor compared to traditional tabletop systems, its adaptability to a range of high-temperature conditions including those in steelmaking environments, and its remote sensing capability. Unlike previous methods such as hotwire thermocouple setups, this system allows for the observation of larger samples, yielding more industrially relevant data. Additionally, background signal filtering of radiant heat has shown improvements in signal-to-noise ratio (SNR). This approach enables the application of Raman analysis in an industrial environment.

This paper investigates the use of an *in-situ* Raman probe for on-line monitoring for molten mould flux at steelmaking temperatures and correlates these measurements with high-temperature viscosity data and chemistry to investigate the underlying structure of these compositions. The findings show that polymeric structures measured using Raman analysis of $CaO\text{-}CaF\text{-}SiO_2\text{-}Al_2O_3$ fluxes are well correlated with viscosity measurements. Additionally, various Raman relative ratios trend with chemistry and basicity. Evidence of the amphoteric nature of alumina can be observed in the measurement of high temperature Raman spectra, particularly in the Al-O-Al bond peak. A ruggedized remote Raman immersion probe has also been developed and demonstrated in an 80 kg foundry induction furnace to showcase suitability for larger industrial environments.

EXPERIMENTAL PROCEDURE

Materials Preparation

The chemical compositions of the fluxes examined in this study are presented in TABLE 1. The flux compositions incorporate CaO/SiO_2 basicity ratios from 0.84 to 1.31 at specific alumina contents of 4.7 wt.% (S-series), 7.5 wt.% (SB-series), 10.0 wt.% (SA-series). To minimize their impact, Na_2O and F contributions to the system were held constant across the samples. Basicity in this study is defined as the ratio of CaO/SiO_2, although other components can be incorporated in the basicity value. The preparation process of the samples was carried out employing laboratory reagent-grade chemicals. Key to achieving the desired chemical accuracy, calcium carbonate and sodium carbonate were carefully measured and added to furnish the necessary CaO and Na_2O contributions. The calcination of these samples was conducted in a controlled vented furnace at 700°C for a duration of 5 hours. This process was crucial for ensuring chemical stability and consistency in the samples. After this calcination, the powdered samples were transferred to an electric furnace and melted at 1300°C. The melting process, lasting between 8 to 10 minutes, was monitored to effectively minimize the loss of volatile components. Upon reaching a molten state, a rapid quenching process was implemented using a large copper block. The quenched glassy samples were catalogued and preserved for the subsequent testing.

TABLE 1 – Chemical composition of synthetic CaO-SiO_2-Al_2O_3 based mold powder flux.

Sample ID	CaO	SiO_2	Al_2O_3	Na_2O	F	CaO/SiO_2
S-1	35.9	42.9	4.7	7.5	9.1	0.84
S-2	39.2	39.5	4.7	7.5	9.1	0.99
S-3	42.2	36.6	4.7	7.5	9.1	1.15
S-4	44.6	34.1	4.7	7.5	9.1	1.31
SA-1	33.5	40.0	10.0	7.5	9.1	0.84
SA-2	36.6	36.8	10.0	7.5	9.1	0.99
SA-3	39.3	34.1	10.0	7.5	9.1	1.15
SA-4	41.6	31.8	10.0	7.5	9.1	1.31
SB-1	34.6	41.3	7.5	7.5	9.1	0.84
SB-2	37.8	38.1	7.5	7.5	9.1	0.99
SB-3	40.6	35.3	7.5	7.5	9.1	1.15
SB-4	43.0	32.9	7.5	7.5	9.1	1.31

In-situ Fibre-Optic Raman System

A significant advancement in this study was the development of a custom-built remote Raman probe, developed and demonstrated by Zhang, B *et al* (2023a). This device was engineered specifically to capture Raman spectra from slags and fluxes in the high-temperature environments typical of steelmaking. The probe's design and functionality were evaluated using two distinct experimental setups. In the first setup, as illustrated in FIG 1, a compact induction heating system equipped with a graphite susceptor, and crucible was employed. This system facilitated the controlled thermal treatment of flux samples, each weighing 2-3 grams. The process commenced with the preheating of the graphite crucible to a target temperature of 1400°C. Following this, the remote Raman probe was deployed to acquire a baseline signal of the radiant heat at this temperature. This baseline acquisition was critical in enhancing the signal-to-noise ratio (SNR) for the subsequent collection of Raman spectra from the flux samples. The procedure for capturing background signals was repeated at various testing temperatures, spanning from 1400°C to 1000°C, at intervals of 50°C. For each temperature setting, quenched glass samples were melted in the crucible, and Raman signals were systematically captured under these controlled conditions. The working distance of the probe head to the molten flux was set to 8 mm to collect the high-temperature Raman spectra. Each sample was

rapidly cooled, typically within 2-3 minutes, due to the small sample size. The time allocated for Raman spectra collection at each temperature was 1-2 minutes to minimize the loss of volatile flux components throughout the testing process. The second experimental setup included an immersible probe tip to allow direct immersion into molten flux, which will be discussed later.

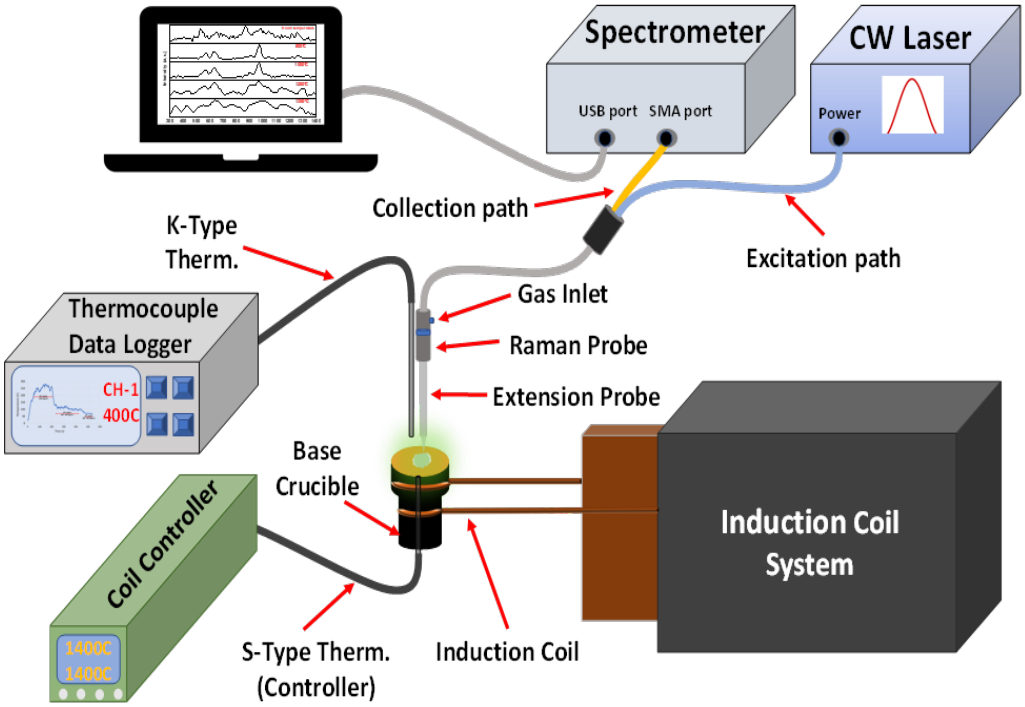

FIG 1 – Schematic of the fibre-optic Raman system combined with an induction coil system for *in-situ* high-temperature experimentation. Induction coil was controlled by an imbedded S-type thermocouple and furnace controller. Ambient probe temperatures were monitored by an external thermocouple. The Raman system is comprised of a remote probe, a continuous-wave (CW) laser, spectrometer, and computer for data collection.

High-Temperature Viscometry

High-temperature viscosity measurements of synthetic mold flux compositions were undertaken. The system utilized a platinum rotational viscometer setup, as delineated in FIG 2. The apparatus consisted of a platinum spindle head designed in accordance with Brookfield® SC4-14 specifications and a custom platinum crucible. The crucible and spindle were placed within a high-temperature molybdenum disilicide furnace. The initial phase of the experiment involved heating the furnace to a temperature of 1400°C. Subsequently, the platinum crucible, loaded with the quenched glass samples, was introduced into the furnace. Upon reaching the molten state, the spindle was carefully lowered into the sample to ensure precise alignment and complete spindle submersion. The rotation speed was set at 50 RPM to satisfy the minimum 10% shear torque requirement of the Brookfield® LV viscometer at the anticipated starting viscosity, thereby ensuring the accuracy of the viscosity measurements. For each viscosity measurement, the temperature was held for approximately 15 minutes at the target temperature for the measurement and reduced in 50°C increments. This procedure was repeated for a temperature range of from 1400°C to 1000°C for all samples, unless flux freezing occurred. The total measurement time for each sample was approximately 2-2.5 hours.

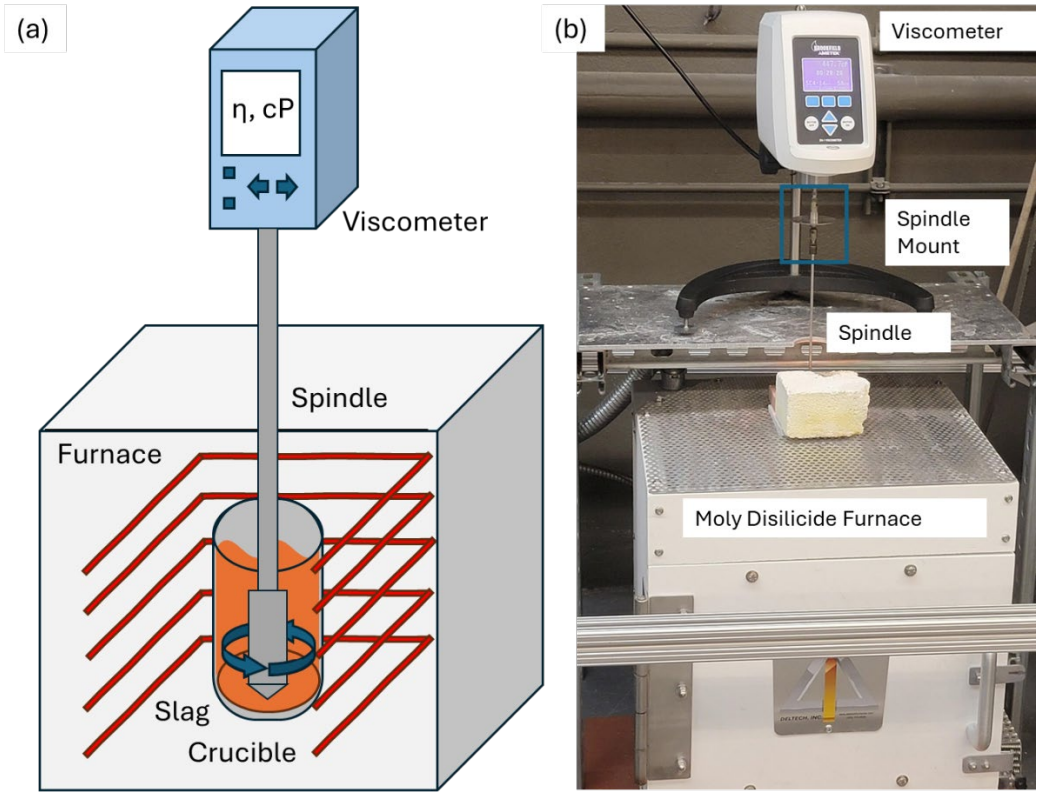

FIG 2 – High-temperature viscometry setup utilizing a platinum spindle and crucible in a moly-disilicide furnace. (a) Diagram of the platinum spindle operating in a furnace. (b) Photograph of a viscometry test of one of four samples presented.

RESULTS AND DISCUSSION

Raman Chemistry Analysis: Alumina & Silica

High-temperature Raman spectroscopy is influenced by thermal radiation, a phenomenon highlighted in the works of Mysen, B.O. and Frantz, J.D. (1992), and McMillan, P.F. et al. (1994). Thermal radiation at high temperatures can interfere with the Raman signal, but if remained constant would allow for its impact to be mitigated in analyses. Zhang, B et al (2023a) proposed a background subtraction technique to address this issue. In the experimental setup, an empty furnace heated to 1400°C provided a baseline for background signal collection. The Raman probe, positioned post-heating, captured this background before introducing the sample for melting. Enhancing signal clarity, the integration time for signal acquisition was set between 1 to 5 seconds, with an averaging of ten sets of spectra per temperature to reduce noise and uncertainty.

The study analysed Raman spectra from twelve melted sample compositions to explore the link between alumina content in mold flux and Raman spectra at high temperatures. Preliminary results of S-series samples at 1400°C are shown in FIG 3, with indicated distinct Raman peaks corresponding to Al-O-Al and Si-O-Si bending vibrations within the 480-560 cm^{-1} and 590-740 cm^{-1} range respectively. Additionally, the Q-region is annotated in the figure. It comprises of four distinct Q^n peaks described in the table as Q^0, Q^1, Q^2, and Q^3. The quantities of nonbridging oxides over number of tetrahedron and the polymeric structure of each is found in the table below.

(a)

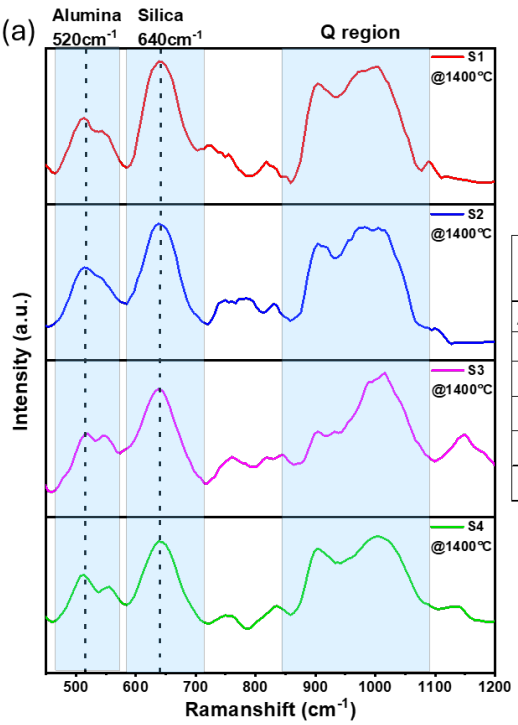

(b)

Name	Peak Raman Shift (cm^{-1})	NBO/T	Polymer Theory
Al-O-Al	480-560	N/A	4-fold ring
Si-O-Si	590-740	N/A	3-fold ring
Q^0	850-880	NBO/T=4	SiO_4 with zero bridging oxygen
Q^1	900-930	NBO/T=3	Si_2O_7 with one bridging oxygen
Q^2	950-980	NBO/T=2	Si_2O_6 with 2 bridging oxygen
Q^3	1040-1060	NBO/T=1	Si_2O_5 with one bridging oxygen

FIG 3 – Original Raman spectra of S-series samples from 400 to 1200 cm^{-1} (a). Regions for alumina, silica, and polymerized Q-region are highlighted. A table (b) containing known peaks, regions of Raman shift, nonbridging oxides/ tetrahedron (NBO/T), polymeric structure. Peak positions are sourced from the works of Gao, J., *et al*. (2016), Wang, W. *et al.* (2020), and Yan, W., *et al.* (2020)

The complex role of Al_2O_3, fluctuating between a network former and modifier, makes it a unique behaviour in these systems, therefore Al_2O_3 and CaO/SiO_2 basicity were the primary independent variables selected for this study. Original spectra measurements are plotted along cumulative, alumina, silica gaussian fits for each plot in FIG 4. The R^2 values are provided for each profile for the cumulative fit to address uncertainty in peak measurements. The minimum R^2 value for all 12 plots was 0.921. Initial observations showed a dual peak behaviour of alumina at low basicity and only resolves when alumina content is sufficient higher. Additionally, at low alumina contents the dual peaking behaviour is prominent with increased twinning at higher basicity. This is believed to be due to the amphoteric nature of alumina as it transitions from network modifier to repolymerizer as the system basicity increases.

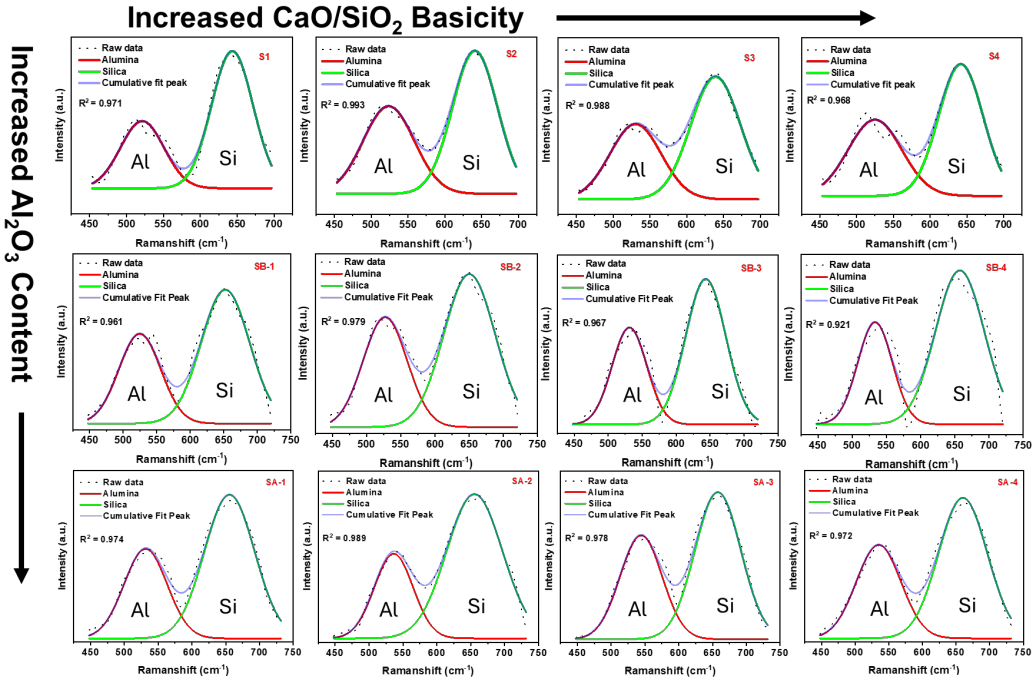

FIG 4 – Raman deconvoluted peak areas of Al-O-Al and Si-O-Si bonds for all 12 samples including S-series (4.7 wt.%), SB-series (7.5 wt.%), and SA-series (10.0 wt.%). All samples were captured at 1350°C.

The general role of alkali oxides such as CaO and Na_2O as network modifiers in silicate structures is well-established. In steelmaking slags, Min, D.J. and Jung, S.B. (2016) and Chen, H. et al. (2016), note that the addition of basic oxides like CaO and Na_2O to a silicate matrix results in the breakdown of Si-O-Si linkages, leading to a more depolymerized and fluid slag. In the CaO-SiO_2-Na_2O system, both CaO and Na_2O act as network modifiers, breaking Si-O-Si bridges in the silica network and creating non-bridging oxygen (NBOs). This process reduces the viscosity of the slag and alters its melting behaviour. Al_2O_3 in a CaO-SiO_2-Al_2O_3 slags can behave both as a network former and a network modifier, depending on the overall composition and the basicity of the slag. When Al_2O_3 is added to a silicate melt, it can participate in the network by substituting for Si^{4+} in the silicate structure, often forming Al-O-Si bridges. However, this substitution requires the presence of a charge-compensating cation, such as Ca^{2+} or Na^{+}, because Al^{3+} has a lower charge than Si^{4+}. In environments with sufficient basic oxides, Al_2O_3 acts more like a network former. The behaviour of Al_2O_3 is significantly influenced by the slag's basicity because of this charge compensation as further discussed in detail by Moretti, R. (2009). Min, D.J. and Jung, S.B. (2016) highlights that understanding the slag composition, including the role of components like Al_2O_3, is crucial for predicting the slag's properties, including viscosity.

To investigate the dual peaks caused by varied alumina content, deconvolution results for samples S-1, SB-1, and SA-1 were adjusted to identify the peak area and positions of alumina-1 and alumina-2 in FIG 5. The results show a convergence of peak position as alumina content increases from 4.7 wt.% to 10 wt.%, ultimately resulting in dual peaks fully blending. At a relatively low basicity of 4.7 wt.%, alumina-1 peak centre was measured at 512 cm^{-1} and alumina-2 peak centre was measured at 552 cm^{-1}. As Al_2O_3 content increased to 7.5 wt.%, the bimodal peaks converged were alumina-1 centre shifted about 4 cm^{-1} and alumina-2 centre shifted 3 cm^{-1}. Lastly, as Al_2O_3 content increased to 10 wt.% the alumina peaks were indifferentiable from one another with a cumulative peak centra around 530 cm^{-1}. All samples maintained a consistent basicity value of 0.84 CaO/SiO_2 ratio. Additional work on this subject can be found by Zhang, B *et al* (2023a).

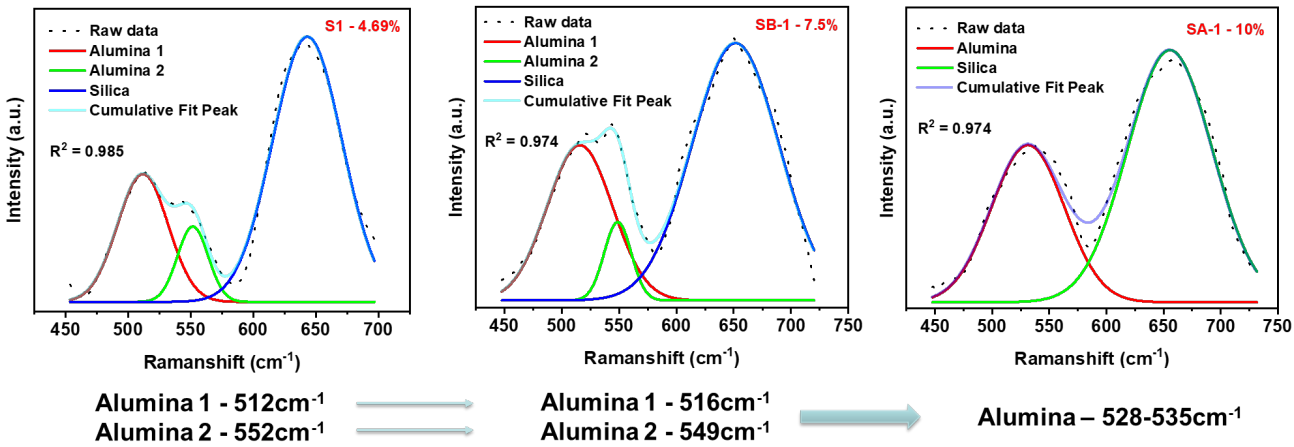

FIG 5 – Raman deconvoluted peak areas of Al-O-Al and Si-O-Si bonds of varied alumina chemistry at a constant CaO/SiO_2 basicity of 0.84. All data was captured at 1350°C.

A NBO is an oxygen atom in a silicate structure that is bound to only one silicon atom, rather than bridging between two silicon atoms. In a typical silicate structure, oxygen atoms usually bridge between two silicon atoms, forming a network. However, when modifiers such as alkaline earth oxides are added, they can break these Si-O-Si bridges, creating non-bridging oxygen. This process results in a more open, less polymerized structure. NBOs are crucial in understanding the properties of silicate glasses and melts, as their presence influences the physical and chemical characteristics of these materials, including viscosity, melting behaviour, and chemical reactivity. In the study by Kim and Sohn (2012), detailed analysis revealed significant structural changes in calcium silicate-

based melts when Al_2O_3 was substituted for SiO_2. The research showed that the introduction of Al_2O_3 led to the formation of more complex aluminosilicate networks, altering the fundamental structure of the melt. As Al_2O_3 content increased, it replaced some of the SiO_2 in the melt structure. This substitution caused a reduction in the number of NBOs due to the formation of Al-O-Si bonds. Al_2O_3 acts differently from SiO_2 in the melt as Al^{3+} ions prefer to be surrounded by four oxygen ions, compared to Si^{4+} ions which are surrounded by four oxygens in a tetrahedral structure in silica. This difference in coordination leads to an increase in the degree of polymerization within the melt.

A valuable aspect of mold flux and slag systems is knowing the basicity. Given that the basicity can vary based on interactions with steel it would be valuable to monitor changes in-line at high temperature. To demonstrate the value of high temperature Raman spectroscopy an inquiry into the correlations of Raman peaks to chemical composition was conducted. Q-region peak height ratios are plotted against compositions of CaO (a), SiO_2 (b), and CaO/ SiO_2 basicity (c) in FIG 6. The Q^3/Q^0 ratio relationship to chemistry shows a stronger correlation than Q^3/Q^2 ratio. This comparison of sheet to monomers of polymerized silica are more closely tied to the overall composition. Since CaO is a depolymerizer, the Q^3/Q^0 ratio decreases as CaO increases. Contrary, SiO_2 polymerizing behaviour is captured by the increasing Q^3/Q^0 ratio as SiO_2 content increases. Overall, this relationship is consistent for CaO/ SiO_2 basicity. This provides one method for correlation of Q-region to chemistry. In addition to these first three plots, all 12 samples, S-series, SB-series, and SA-series with increasing contents of Al_2O_3, were investigated to show the relationship of Al-O-Al and Si-O-Si relative peak ratios. Using peak height measurements of the Al-O-Al and Si-O-Si peaks centred in the regions of 535 cm-1 and 655 cm-1 respectively, a relationship was found correlating relative peak height ratios to compositional ratios that can be found in FIG 6 (d – f). Across a range of CaO/ SiO_2 basicity of 0.84 to 1.31, the SiO_2 content correlates with the Al-O-Al and Si-O-Si relative ratios. As SiO_2 content increases the measured Raman peak ratio decreases, providing a means to predict SiO_2 content across a wide range of basicity. Additionally, as CaO/SiO_2 basicity increases, the Al-O-Al/Si-O-Si peak ratio increases. Overall, the trend shows a consistent structural change that occurs due to basicity changes. The increase in basicity means there are more Ca^{2+} and potentially Al^{3+} cations to depolymerize the silicate network resulting in breakage of more Si-O-Si bonds resulting in reduced peaks in Raman spectra. The deviations across groups of S, SB, and SA samples are attributed to the amphoteric nature of Al_2O_3 as basicity transitions from an acidic to a basic mold flux. This trend with Al-O-Al/Si-O-Si ratio holds true to the overall basicity of the composition as the ratio of peaks increase alongside the overall basicity in a linear trend. It is believed that the combined relationships of the Al-O-Al, Si-O-Si, and Q-region peaks could yield an indiscriminate method to detect in-situ chemistry.

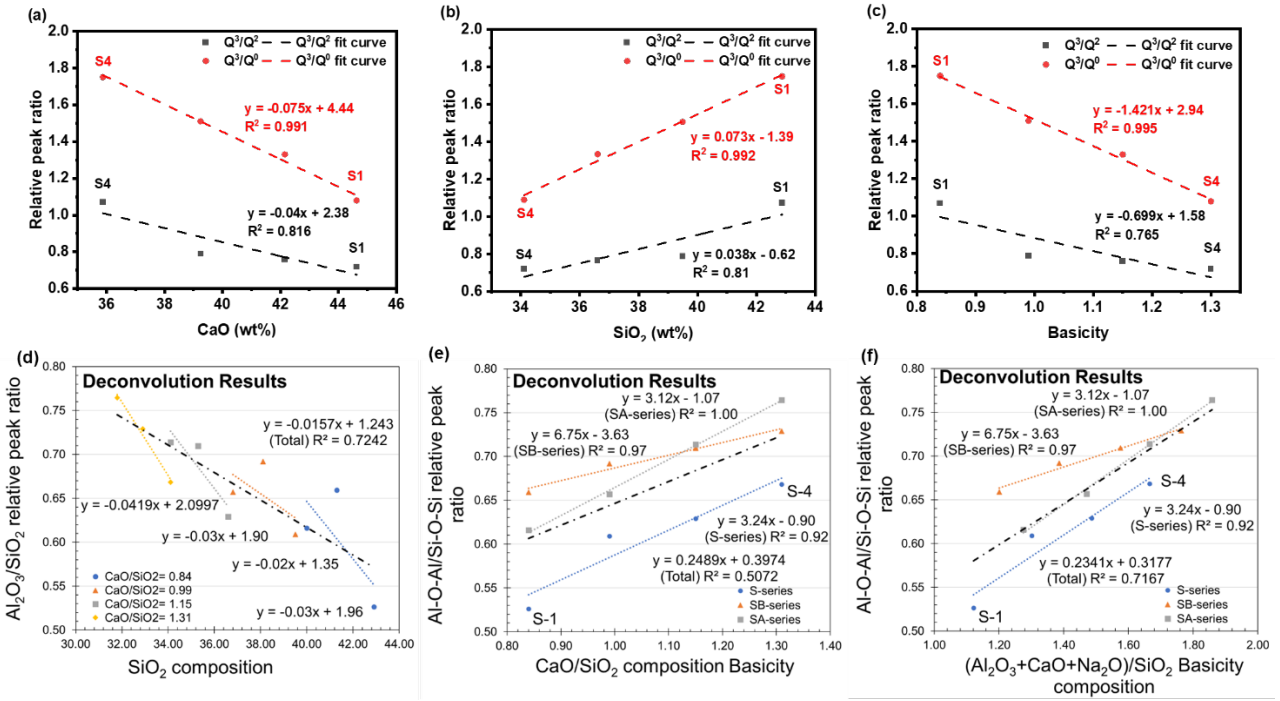

FIG 6 – Raman deconvoluted relative peak height ratios of Al-O-Al, Si-O-Si, and Q-region correlated with stochiometric chemical composition. This includes Q-region to CaO (a), SiO_2 (b), and CaO/SiO_2 basicity (c). Additionally, Al-O-Al and Si-O-Si peak height relative ratios are correlated to SiO_2 (d), CaO/SiO_2 basicity ratio (e), and $(Al_2O_3+CaO+Na_2O)/SiO_2$ basicity ratio (f).

The peak intensities are tied to bond vibrations and increase in frequency and intensity based on the chemical composition. The peaks correspond to specific bond types and arrangements, such as Si-O-Si in silicates or Al-O-Al in aluminates. As greater quantities of chemical bonds exist in the mixture, a greater intensity of generated Raman signal from these bonds is produced. As a result, the relative peak intensities provide valuable information as to the overall composition. In order to normalize the arbitrary units per individual samples, relative ratios must be used. Since each peak in the same spectra is signal processed under the same conditions it is appropriate to compare and ratio peaks within the sample. To compare spectra from different samples relative ratios must be used to identify changes in intensities.

Raman Analysis of Viscosity Temperature Dependance

The primary focus in this study is investigating the *in-situ* high-temp Raman spectra for sample SA-1. Nine Raman spectra from nine temperature conditions are performed, as shown in FIG 7 and 8. The temperature dependence of viscosity has been well documented in literature notably in McMillan, P.F. et al. (1994), Daniel, I. et al. (1995) and Zhang, B. et al. (2023a). To compare the range of viscosity measurements to Raman, a comprehensive analysis of Raman spectra across the range of temperatures was performed. Deconvolution of Raman spectra is a sophisticated analytical technique used to resolve complex Raman signals into individual components that are tied to specific molecular linkages. Through deconvolution overlapping peaks can be separated and quantified. Previously described bonds such as Al-O-Al (530 cm^{-1}) and Si-O-Si (650 cm^{-1}) have well known positions that provide conditions for measurement. In addition to these individual peaks, a large overlapping region of peaks can be identified from 850 to 1100 cm^{-1} typically described as the Q-region. The Q-region contain peaks generated from various polymerized stated of silica. It is these peaks that provide the most value when interpreting the structure of liquid slags and mold fluxes and their viscosity behaviour. For this reason, the Raman spectra of the Q-region was focused and underwent baselining and deconvolution techniques to identify area peaks by gaussian approximation. Peak feature positions are defined within a tight range based on consensus in documented literature findings. Known peak positions were identified and supported by reference literature found in the works of Gao, J., *et al*. (2016), Wang, W. *et al.* (2020), and Yan, W., *et al.* (2020). Resulting figures can be found in FIG 8.

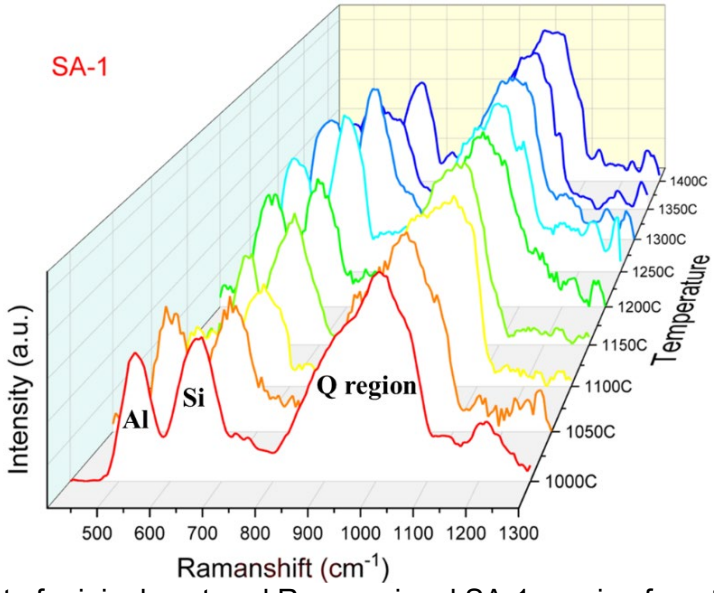

FIG 7 – Waterfall plot of original captured Raman signal SA-1 ranging from temperature 1400°C (back) to 1000°C (front). Significant regions include spectral peaks for Al-O-Al 530 cm^{-1}, Si-O-Si around 650 cm^{-1}, and the Q region spanning from 850 to 1100 cm^{-1}.

The Q-region comprises of a multitude of various peaks depending on the composition in question. In this sample case there are believed to be 4 polymerized silica states. All nine samples have successfully deconvoluted for four individual peaks, as shown in FIG 8. Each peak was represented by Q^0 - SiO_4 - Monomer; Q^1 - Si_2O_7 – dimer; Q^2 - SiO_3 – chain; Q^3 - Si_2O_5 - sheet. In Raman spectroscopy applied to silicate systems, the Q-region is a vital part of the spectrum. This region represents the polymerized silica (SiO_4) tetrahedron. This region is key to understanding silicate material structures, revealing the degree of polymerization of the silica network through distinct peaks associated with different silica structures, known as Q^n species, where 'n' indicates the number of bridging oxygen atoms. For instance, the Q^0 species, or monomer, represents isolated SiO_4 tetrahedra with no bridging oxygens, or all being non-bridging. The Q^0 species is typically measured from 850 to 880 cm-1. The Q^1, or the dimer form, consists of two SiO4 tetrahedra connected by a single bridging oxygen, with its presence in the range of 900 to 930 cm-1. The Q^2, or chain structure, where each SiO_4 tetrahedron shares two bridging oxygens with its neighbours, forming chain-like configurations, also shows distinct peaks in the range of 950 to 980 cm-1. The Q^3, or sheet structure, involves each SiO_4 tetrahedron linking to three others via bridging oxygens, forming sheet-like structures, and is detectable in the Raman spectra from 1040 to 1060 cm-1. Overall, a strong fit was established for all spectra with R^2 values greater than 0.958 for the combined gaussian fit. Transitions between relative peak sizes can be observed when temperature is varied, specifically Q^2 and Q^3 peaks were predominant to Q^0 and Q^1 at lower temperatures.

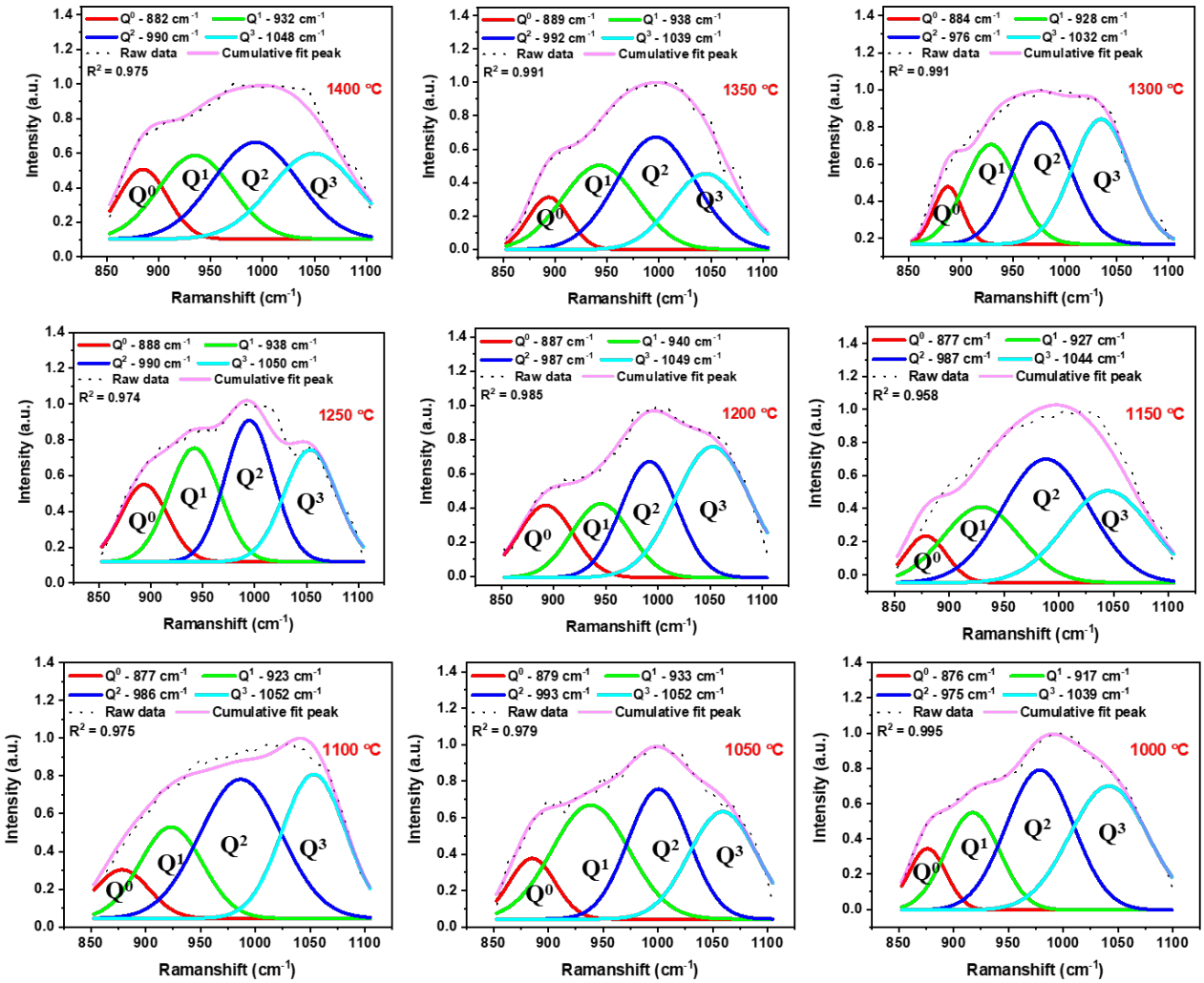

FIG 8 – Deconvoluted Raman spectra of SA-1 samples at 9 testing temperature conditions from top left (1400°C) to bottom right (1000°C). A range of 800 to 1150 cm^{-1} is shown to illustrate the deconvolution results of Q-region.

The viscosity data compiled for the SA-1 to SA-4 samples show consistency, evident in the repeatability of measurements under both cooling and heating conditions seen in FIG 9. Viscosity measurements were plotted linearly as the inverse of temperature vs the natural log of viscosity

measured. This is due to the typical Arrhenius behaviour of viscosity and temperature. Similar works have illustrated this behaviour in detail including Chen, H. (2017), and Wan, X. *et al.* (2024). The Arrhenius equation profiles well as temperature increases in slag and mold flux systems the viscosity, measured in centipoise, decreases at an exponential rate. For this reason, linear regression lines were used to support this and to measure an activation energy for the profile. Furnace temperature uniformity had minimal impact on measurement accuracy is shown by the high R^2 results being equal to or greater than 0.986 for all four samples. Instead, the precision of measurements was more significantly influenced by the alignment of the spindle, as observed during the early testing of sample SA-1 where realignment of the viscometer setup was necessary. The overall profiles of viscosity data align well with the exponential Arrhenius behaviour observed in other studies, suggesting a commonality in the rheological properties of such slag materials.

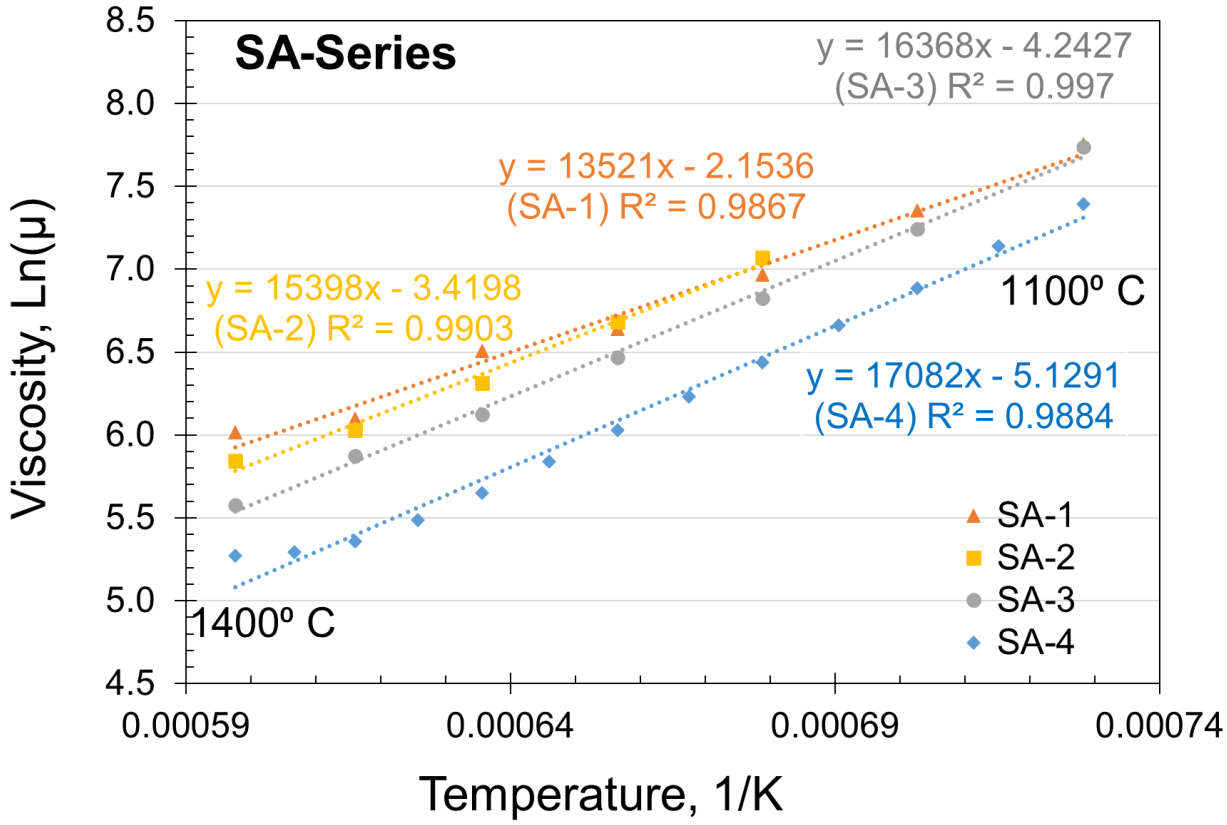

FIG 9 – High-temperature viscometer data collected for samples SA-1, SA-2, SA-3, and SA-4 from 1400°C to 1100°C.

In similar works by Kim and Sohn (2012), increased polymerization and structural complexity of the melt, resulting from higher Al_2O_3 content, had a direct impact on the physical properties of the melt, notably its viscosity. The melt became more viscous with increasing Al_2O_3, attributed to the enhanced polymerization and the formation of a more interconnected network structure. This observation was also consistent with FIG 9, samples behaved more viscous-like increasing as the Al_2O_3/SiO_2 ratio increased across the samples SA-1 to SA-4. It is important to address that this was observed at high temperatures where precent solids are at relatively low quantities. As temperatures are reduced, overlap of the viscosity vs temperature trend can be seen were the influence of solid fractions play a more prominent role. Further analysis of these forming crystallite is needed to address their impact on viscosity.

To further analyse the relationship between Raman spectra and viscosity of mold flux samples, the peak area measurement is investigated for a correlation. According to the nature of the polymerized network, higher order Q^n provides the silicate structure with larger sized linkages which are less prone to mobility, leading to a more viscous mixture. To index the total polymerized silica structure measured from the Raman spectra, an equation, Eq. 1 was constructed.

$$[(X_1*Q^1) + (X_2*Q^2) + (X_3*Q^3)]/(X_0*Q^0) \quad \text{(Eq. 1)}$$

In the proposed model expressed by Eq. 1, each observable Q^n nomenclature is assigned a coefficient. The assignment is based on the relative molecule sizes of each polymerized state, with a basic increasing geometric ratio designated for each X_n. Then, based on the model discussed above, the results of $[(X_1*Q^1) + (X_2*Q^2) + (X_3*Q^3)]/(X_0*Q^0)$ was used to correlate with the measured viscosity, as shown in FIG 10. Since Q^0 represents a monomer, X_0 is assigned a value of 1. For subsequent X_n values, an increase by factors of two or more is applied as a baseline for optimization. Optimizing the X_1, X_2, and X_3 values involves utilizing an adjusted R^2 value as a response, with adjustments made through a sequential quadratic programming (SQP) script in MATLAB®. The optimized values of X_1, X_2, and X_3 are then used to construct FIG 10, adhering to predefined bound constraints of $X_0=1$, $1< X_1 < X_2 < X_3$. This was later modified to $X_1=1.5$, $X_2=2$, and $X_3=12$ to retain the geometric progression which better fits the sizes of Q^n. The most significant impact on the response was observed when minimizing X_1 and X_2 while maximizing X_3. This implies that the Q^3 (sheet) has a greater impact to viscosity compared to Q^1 (dimmer), and Q^2 (chain) structures based on the weighted sum of Q^n. A linear regression fit is plotted using the natural logarithm of measured viscosity as a response variable. An R^2 of 0.89 was achieved using the methods previously described. The Q^3/Q^0 relationship still holds the strongest correlation to viscosity, suggesting the dominant contribution to viscous properties of molten mold flux systems is the Q^3 sheet of SiO_4 tetrahedron. However, further work is required to enhance the robustness and accuracy of Equation 1 and its X_n values, ensuring a more reliable and comprehensive understanding of the contributions of the various Q^n to the overall structure of the composition. Particularly, expanding the data set to incorporate SA-2, SA-3, SA-4 and additionally a S-series of samples containing a lower Al_2O_3 content of 4.7 wt.%. The existence of Al-O-Si bonds near the Q-region have been reported in works aforementioned, but no evidence of their presence has been found in the proposed samples in this study. Using this proposed model, a method for predicting viscosity based on the measured in-situ high temperature Raman spectra is proposed. This provides a valuable tool for process control for industrial steelmaking environments.

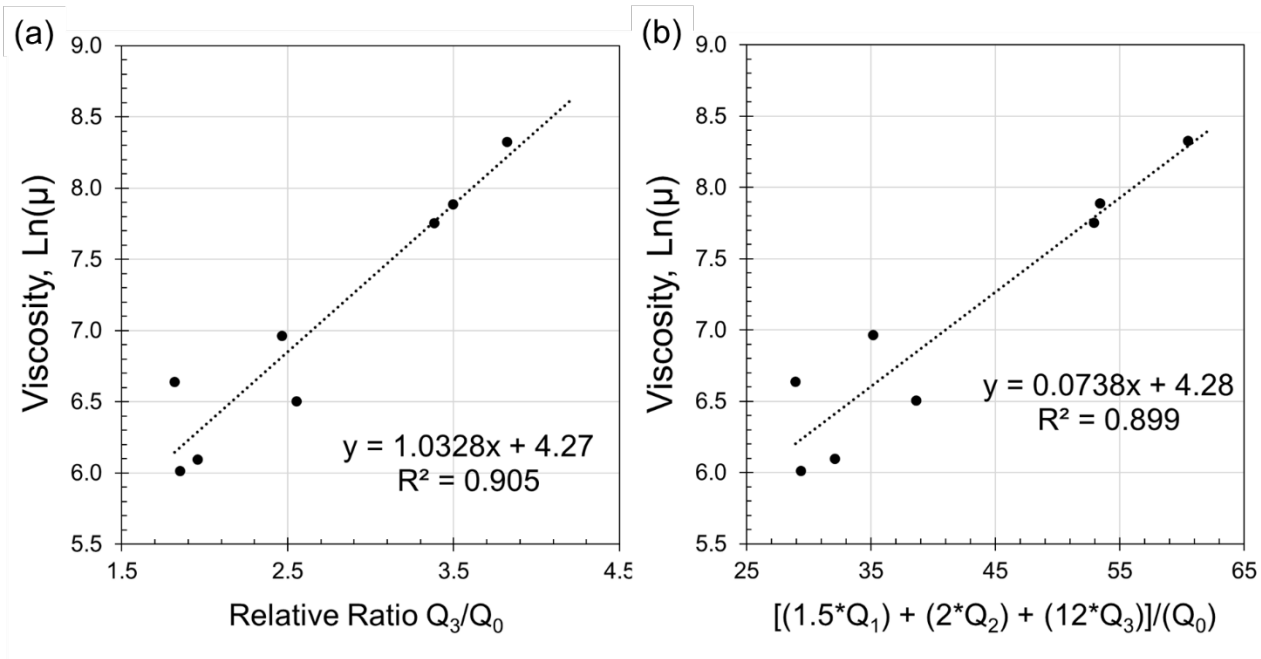

FIG 10 – Quantified Q-region formula for predicting viscosity using data from SA-1 going from 1400°C to 1100°C. A comparison of Q^3/Q^0 ratio (a) and Eq. 1 (b) can be seen in the figure above.

The interplay between depolymerization and viscometry in silicate melts is a complex but critical aspect of understanding the behaviour of these materials under molten conditions. Raman spectroscopy serves as a powerful tool in deciphering the molecular dynamics that underlie these changes. The insights gained from these studies are valuable in numerous scenarios in metallurgical processes, where control over melt properties is essential.

Raman Immersion Dip Test

To enhance the methodology presented, a ruggedized Raman probe was developed and demonstrated for larger-scale dip testing. This probe, capable of short-duration dips of 30 sec or more in steelmaking environments, features improvements like a telescopic extension lens and air-cooling channels in its copper housing This ensures an effective working distance and improves probe protection. An apparatus for dip testing has been created to enable highly precise position control, adjustable within 1-3 mm. Complementing this, a molybdenum viscometry setup is in development to address complex industrial mold flux compositions, which are not suitable for the existing platinum viscometry setup due to platinum-iron embrittlement. A large-scale experimental setup, illustrated in FIG 11, simulates an industrial-scale environment. This includes a 90 kg steel induction melting furnace, designed to handle large quantities of steel and mold powder flux samples. The setup's centrepiece is the enhanced version of the remote Raman probe, encased in a custom-designed copper block with air-cooling channels. This design is critical for protecting the probe from the furnace's extreme temperatures and harsh conditions. The telescopic lens, extending the working distance to 3 cm reducing contact and proximity to the molten flux/slag. Additionally, the cooling system's exhaust gas is used to create a positive pressure environment at the probe tip, effectively preventing slag or steel from entering the probe body and thus reducing damage risk.

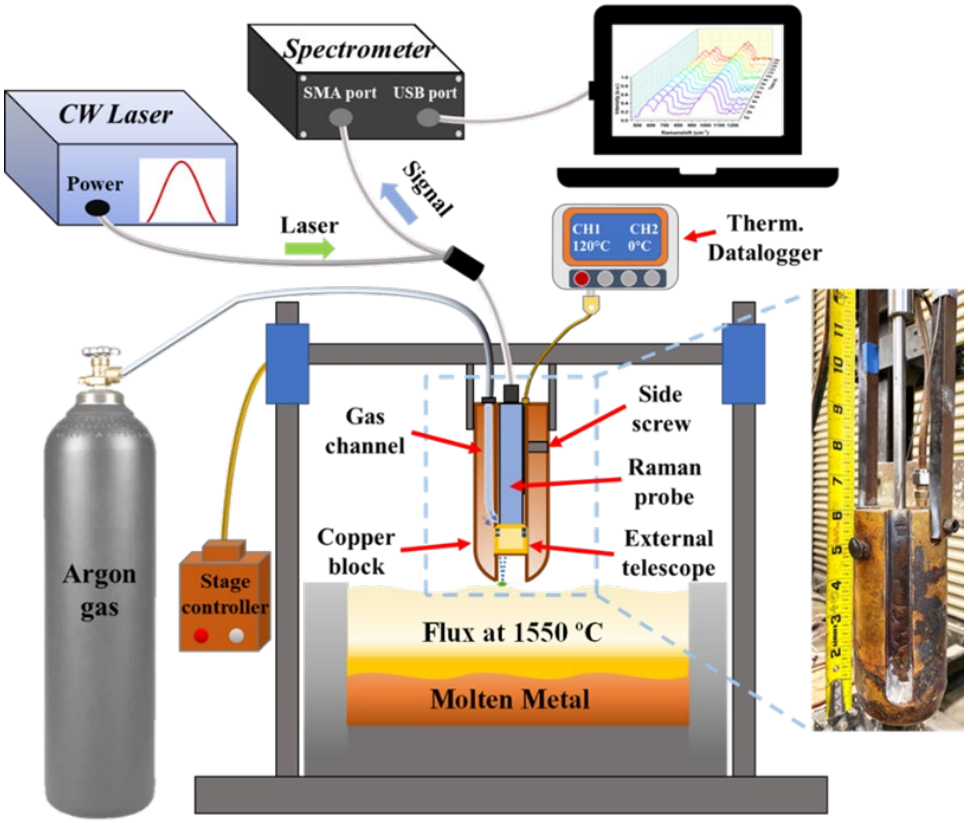

FIG 11 – Industrial foundry mold flux dip testing setup with ruggedized Raman probe. Raman system includes continuous wave (CW) laser, spectrometer, computer, and probe. Ruggedized Raman probe housing including argon gas cooling is mounted to a motorized dipping stage.

The housing is attached to an automated dip tester, managed by a programmable logic controller (PLC), which offers meticulous control over the dipping depths. The melting process in the induction furnace highlighted challenges like natural convection, leading to the liquid mold powder flux accumulating around the furnace's perimeter and forming thinner layers of suspended flux. In conclusion, the development of a suitable high-temperature viscometry setup for FeO-bearing slags and fluxes, alongside the larger scale dip tests, aims to provide comprehensive viscosity and Raman data. This data will assist in proving the scalability of the proposed methodology. Moving forward, a model for various mold flux compositions is being prepared for an industrial caster dip test, aiming to fully demonstrate the Raman probe's suitability in practical steelmaking applications. Future work is planned to enhance and further evaluate the ruggedized Raman probe dip testing setup, aiming to facilitate longer duration dips and potentially yield more comprehensive data of exchange

reactions between steel and molten mold flux. This improvement is expected to provide a deeper insight into the flux's behaviour under varied operational conditions.

CONCLUSIONS

In this study, the development and application of a remote fibre-optic Raman probe for real-time analysis of steelmaking slag and mold flux compositions at elevated temperatures has been demonstrated. The research combined *in-situ* Raman spectroscopy with high-temperature viscosity data to elucidate the underlying structural behaviours in CaO-CaF-SiO_2-Al_2O_3 based systems. Experimental procedure for high-temperature viscometry and Raman spectra collection was demonstrated. The deconvolution of overlapping peaks in the alumina, silica, and Q-region of the Raman spectra enabled a clearer understanding of the high-temperature structural features. This deconvolution was key in correlating Raman spectral features to chemical composition, particularly (Al_2O_3/SiO_2) ratio to SiO_2 content and (Al_2O_3+CaO+Na_2O)/SiO_2 basicity. Furthermore, viscosity measurements were explained by Raman deconvoluted Q-region as the degree of polymerization in the silicate network dictated structure. The results underscored the reliability of Raman spectroscopy in predicting synthetic mold flux viscosity, particularly with Q^3/Q^0 ratio as other more comprehensive Q^n calculations could not achieve a better fit. This illustrates how Q^3 is the predominant feature in the Raman Q-region tied to the underlining structure including viscosity. This observation aligns with the understanding that larger polymeric linkages, such as Q^3 (sheet), have a more substantial impact on viscosity compared to smaller linkages like Q^1 (dimmer), and Q^2 (chain). The research concluded that the Raman spectra of CaO-CaF-SiO_2-Al_2O_3 based mold flux systems exhibit fundamental behaviours closely related to the structure of these compositions, influencing both the Raman spectra and viscosity measurements. This study not only contributes to the field of metallurgy by providing a deeper understanding of the structural dynamics of mold fluxes and slags but also offers a practical approach for real-time monitoring and control of these materials in various industrial settings. The integration of Raman spectroscopy with viscometry presents a powerful tool for advancing our understanding of material properties under extreme conditions, with significant implications for improving industrial processes and material design.

ACKNOWLEDGEMENTS

This research was funded by the U.S. Department of Energy’s Office of Energy Efficiency and Renewable Energy (EERE)under the Advanced Manufacturing Office (AMO) Awards DE-EE0009392 and DE-EE0009119. The views and opinions of authors expressed herein do not necessarily state or reflect those of the United States Government or any agency thereof. Additional support was provided by the Peaslee Steel Manufacturing Research Center (PSMRC) at Missouri University of Science and Technology.

REFERENCES

Chen, H. et al. (2016) 'Structure studies of silicate glasses by Raman Spectroscopy,' in Springer eBooks, pp. 175–182. https://doi.org/10.1007/978-3-319-48769-4_18.

Chen, H. (2017) Viscosity studies of High-Temperature metallurgical slags relevant to ironmaking process. https://doi.org/10.14264/uql.2017.995.

Daniel, I. et al. (1995) 'In-situ high-temperature Raman spectroscopic studies of aluminosilicate liquids,' Physics and Chemistry of Minerals, 22(2). https://doi.org/10.1007/bf00202467.

Gao, J., Wen, G., Huang, T., Tang, P., et al. (2016) 'Effects of the composition on the structure and viscosity of the CaO–SiO2-based mold flux,' Journal of Non-Crystalline Solids, 435, pp. 33–39. https://doi.org/10.1016/j.jnoncrysol.2016.01.001.

Gao, J., Wen, G., Huang, T. and Tang, P. (2016a) 'The structure and the crystallization behaviour of the CAO-SIO2-AL2O3-Based mold flux for High-Al Steels casting,' in Springer eBooks, pp. 291–298. https://doi.org/10.1007/978-3-319-48769-4_31.

Gyakwaa, F. et al. (2019) 'Applicability of Time-Gated Raman Spectroscopy in the characterisation of Calcium-Aluminate inclusions,' Isij International, 59(10), pp. 1846–1852. https://doi.org/10.2355/isijinternational.isijint-2019-122.

Gyakwaa, F., Aula, M., Vuolio, T., et al. (2020) 'Characterization of multiphase mixtures of calcium aluminates and magnesium aluminate spinel using Time-Gated RAMAN spectroscopy,' Steel Research International, 91(8). https://doi.org/10.1002/srin.202000084.

Gyakwaa, F., Aula, M., Alatarvas, T., Shu, Q., et al. (2020a) 'Quantification of Synthetic Nonmetallic Inclusion Multiphase Mixtures from a CaO–Al2O3–MgO–CaS System Using Raman Spectroscopy,' Steel Research International, 92(1). https://doi.org/10.1002/srin.202000322.

Gyakwaa, F., Aula, M., Alatarvas, T., Vuolio, T., et al. (2020b) 'Application of Raman spectroscopy for characterizing synthetic Non-Metallic inclusions consisting of calcium sulphide and oxides,' Applied Sciences, 10(6), p. 2113. https://doi.org/10.3390/app10062113.

Gyakwaa, F., Aula, M., Alatarvas, T., Vuolio, T., et al. (2020c) 'Characterisation of binary phase mixtures of Magnesium-Aluminate spinel and Calcium-Aluminates using Time-Gated Raman spectroscopy,' Isij International, 60(5), pp. 988–997. https://doi.org/10.2355/isijinternational.isijint-2019-576.
Kim, G.H. and Sohn, I. (2012) 'Effect of Al2O3 on the viscosity and structure of calcium silicate-based melts containing Na2O and CaF2,' Journal of Non-Crystalline Solids, 358(12–13), pp. 1530–1537. https://doi.org/10.1016/j.jnoncrysol.2012.04.009.
Malfait, W.J. and Halter, W.E. (2008) 'Structural relaxation in silicate glasses and melts: High-temperature Raman spectroscopy,' Physical Review B, 77(1). https://doi.org/10.1103/physrevb.77.014201.
Malfait, W.J., Zakaznova-Herzog, V.P. and Halter, W.E. (2007) 'Quantitative Raman spectroscopy: High-temperature speciation of potassium silicate melts,' Journal of Non-Crystalline Solids, 353(44–46), pp. 4029–4042. https://doi.org/10.1016/j.jnoncrysol.2007.06.031.
McMillan, P.F. et al. (1994) 'A study of SiO2 glass and supercooled liquid to 1950 K via high-temperature Raman spectroscopy,' Geochimica Et Cosmochimica Acta, 58(17), pp. 3653–3664. https://doi.org/10.1016/0016-7037(94)90156-2.
Mills, K.C. (2016) 'Structure and properties of SLAGS used in the continuous casting of steel: Part 1 Conventional mould powders,' Isij International, 56(1), pp. 1–13. https://doi.org/10.2355/isijinternational.isijint-2015-231.
Min, D.J. and Jung, S.B. (2016) 'Current status of slag design in metallurgical processes,' in Springer eBooks, pp. 17–28. https://doi.org/10.1007/978-3-319-48769-4_2.
Moretti, R. (2009) 'Polymerisation, basicity, oxidation state and their role in ionic modelling of silicate melts,' Annals of Geophysics, 48(4–5). https://doi.org/10.4401/ag-3221.
Mysen, B.O. and Frantz, J.D. (1992) 'Raman spectroscopy of silicate melts at magmatic temperatures: Na2O-SiO2, K2O-SiO2 and Li2O-SiO2 binary compositions in the temperature range 25–1475°C,' Chemical Geology, 96(3–4), pp. 321–332. https://doi.org/10.1016/0009-2541(92)90062-a.
Pretorius, E.B. (2020) 'The role of transient slags in steelmaking,' AISTech2020 Proceedings of the Iron and Steel Technology Conference [Preprint]. https://doi.org/10.33313/380/066.
Wan, X. et al. (2024) 'Insight into compositional dependence of thermophysical properties and structure of Al2O3-SiO2-CaF2-CaO-Li2O melts,' Journal of Non-Crystalline Solids, 626, p. 122807. https://doi.org/10.1016/j.jnoncrysol.2023.122807.
Wang, W. et al. (2020) 'Viscosity and structure of MgO–SiO2-based slag melt with varying B2O3 content,' Ceramics International, 46(3), pp. 3631–3636. https://doi.org/10.1016/j.ceramint.2019.10.082.
Yan, W., Zhang, G. and Li, J. (2020) 'Viscosity and structure evolution of CaO–SiO2-based mold fluxes with involvement of CaO–Al2O3-based tundish fluxes,' Ceramics International, 46(9), pp. 14078–14089. https://doi.org/10.1016/j.ceramint.2020.02.208.
Zhang, B., Tekle, H., O'Malley, R.J., Sander, T.P., et al. (2023a) 'In situ and Real-Time mold flux analysis using a High-Temperature Fiber-Optic Raman sensor for steel manufacturing applications,' Journal of Lightwave Technology, 41(13), pp. 4419–4429. https://doi.org/10.1109/jlt.2023.3239428.
Zhang, B., Tekle, H., O'Malley, R.J., Smith, J.D., et al. (2023) 'In situ High-Temperature raman spectroscopy via a remote Fiber-Optic raman probe,' IEEE Transactions on Instrumentation and Measurement, 72, pp. 1–8. https://doi.org/10.1109/tim.2023.3244238.
Zhang, B., Tekle, H., O'Malley, R.J., Sander, T.P., et al. (2023b) 'Structural analysis of molten materials by a remote fiber optic Raman sensor,' Optical Waveguide and Laser Sensors II, 12532. https://doi.org/10.1117/12.2663853.
Zhang, R. et al. (2020) 'Structure and viscosity of molten CAO-SIO2-FEXO slag during the early period of basic oxygen steelmaking,' Metallurgical and Materials Transactions B-process Metallurgy and Materials Processing Science, 51(5), pp. 2021–2029. https://doi.org/10.1007/s11663-020-01888-8.